Wang and Lu *Protection and Control of Modern Power Systems* (2018) 3:7
https://doi.org/10.1186/s41601-018-0080-6

Protection and Control of Modern Power Systems

ORIGINAL RESEARCH Open Access

Design optimization of hydraulic energy storage and conversion system for wave energy converters

Dong Wang* and Kaiyuan Lu

Abstract

Wave energy collected by the power take-off system of a Wave Energy Converter (WEC) is highly fluctuating due to the wave characteristics. Therefore, an energy storage system is generally needed to absorb the energy fluctuation to provide a smooth electrical energy generation. This paper focuses on the design optimization of a Hydraulic Energy Storage and Conversion (HESC) system for WECs. The structure of the HESC system and the mathematical models of its key components are presented. A case study and design example of a HESC system with appropriate control strategy is provided. The determination of the ratings of the HESC system is also investigated in order to achieve optimal system energy efficiency.

Keywords: Energy storage, Hydraulic system, Wave energy, System modelling, System optimization

1 Introduction

As a kind of renewable energy, wave energy and its utilization have obtained increasing interests in the past decade [1–4]. Wave Energy Converter (WEC) is normally used to harvest the wave energy and transform it to electrical energy. Many different WEC systems have been studied and reported [1–8], and they can be categorized into two main types as turbine-type and buoy-type [1]. The turbine-type WECs, including Oscillating Water Column (OWC) WEC [4] and overtopping WEC [5, 6], use turbines as the main energy conversion device. While the buoy-type WECs, which are also known as Point Absorber (PA) WECs, utilize fully submerged (below surface) absorber (e.g. the Archimedes Wave Swing (AWS) based [7]) or floating (on the surface) absorber [8–10] to capture the wave energy. The PA-WECs are considered to be more environmental friendly [1] and have obtained interests from both academic researches [7–10] and industrial prototypes [11, 12].

The Power Take-Off (PTO) systems of the PA-WECs can be categorized into two main types as electric-type and hydraulic-type [3]. The electric PTOs, including linear generator [7, 10] and rotary generator with gearbox [9], directly convert the captured wave energy to electricity. While the hydraulic PTOs transfer the wave energy to hydraulic energy, which is used to drive either a turbine [13] or a hydraulic motor [8] that is connected to an electric generator.

The situation of waves with large force at low speed can be well suited by the hydraulic PTOs since they can provide much larger force density than the electric PTOs, especially at high system pressure [2]. Thus, hydraulic PTOs should be more compact in size and weight, economically competitive, and relatively easy to install and maintain [2, 14]. Furthermore, since the wave energy is highly fluctuating, from both the wave-to-wave and wave states time scales, the required peak power capacity of the PTOs greatly exceeds the time-averaged power delivered to the grid. Energy storage system is thus generally required to smoothen the final electrical power output to avoid the impairment of power quality from the grid point of view [3, 14]. In order to reduce the power ratings of the key components of the PTO for achieving a compact and energy efficient design, the energy storage device is expected to be located directly after the wave energy absorbers. The gas accumulator, which stores the hydraulic energy and fluid by compressing the gas, is currently the most common choice [2, 3, 14].

* Correspondence: dwa@et.aau.dk
Department of Energy Technology, Aalborg University, Pontoppidanstraede 111, DK-9220 Aalborg, Denmark

In this paper, the design optimization of the Hydraulic Energy Storage and Conversion (HESC) system used in the hydraulic PTO system for PA-WECs is presented. The ratings of the HESC system are investigated in order to optimize the system energy efficiency. This paper is organized in the following manner. Section 2 illustrates the structure of the HESC system for PA-WECs and the mathematical models of all the key components are presented. In Section 3, the integration of the HESC system in the WEC is discussed and its performance is illustrated. Design optimization of the HESC system regarding energy efficiency is carried out and system design guidelines are provided in Section 4. Finally, Section 5 draws conclusion.

2 HESC system modelling

Figure 1 illustrates the structure of the HESC system that can be adopted in WECs. It consists of high-pressure gas accumulator, hydraulic motor, low-pressure reservoir, pipelines, and electrical generator. The gas accumulator absorbs the fluctuating flow from the hydraulic input and provides required flow to drive the variable displacement swash-plate hydraulic motor and the connected electrical generator at certain power level. A pressure relief valve is used to protect the system against over-pressure. The energy overflow can be collected by another energy storage system, which can be shared by several PTOs. The fluid loss caused by the overflow is compensated by the backflow to maintain the pressure in the reservoir. The mathematical models of the key components are given in details in this section.

2.1 Gas accumulator

The connection interface between the accumulator and the hydraulic system can be described by two variables: the actual flow rate of the fluid entering the accumulator Q_a and the fluid pressure at the accumulator inlet p_a.

Since the accumulator stores the hydraulic fluid by compressing the gas in it, the actual flow rate of the fluid entering the accumulator Q_a is equal to the compression rate of the gas in the accumulator

$$Q_a = -m_g \frac{dv}{dt}, \tag{1}$$

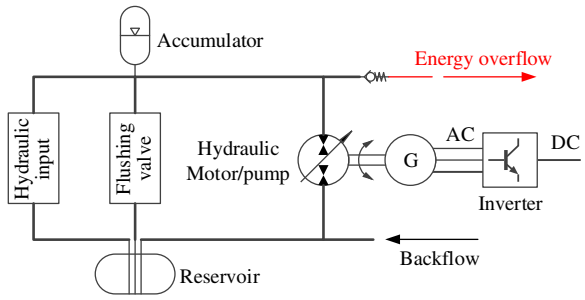

Fig. 1 Hydraulic energy storage and conversion system

where t is the time, m_g is the gas mass, and v is the gas specific volume. The gas specific volume can be calculated by integrating both sides of (1) if the initial gas specific volume v_0 is known.

The accumulator inlet pressure p_a is determined by the gas absolute pressure p_g and the pressure difference between them. The gas absolute pressure p_g can be calculated according to the Benedict-Webb-Rubin (BWR) equation of state as

$$p_g = RT/v + \left(B_0RT - A_0 - C_0/T^2\right)/v^2 + a\alpha/v^6 + (bRT - a)/v^3 + \left(C\left(1+\gamma/v^2\right)e^{-\gamma/v^2}\right)/v^3T^2, \tag{2}$$

where A_0, B_0, C_0, a, b, c, α, and γ are constants in BWR equation, and T is the gas temperature. In this analysis, nitrogen is considered.

Gas temperature T varies during the compression and expansion process and it will cause irreversible heat transfer, i.e. from gas to accumulator wall and eventually to the outside environment. Elastomeric foam with appropriate properties is inserted to perform as "heat sink" and the thermal loss can be reduced significantly. Since the foam has large contacting surface with gas and very small wall thickness, it is appropriate to assume that the foam and gas are at the same temperature T all the time [15]. Thus, the gas energy equation can be written based on the energy balance principle as

$$m_g \frac{du}{dt} = -p_g \frac{dV}{dt} - m_f c_f \frac{dT}{dt} - hA_w(T - T_w), \tag{3}$$

where u is the gas internal energy per unit mass, V is the gas volume, m_f is the foam mass, c_f is the specific heat of foam, h is the heat transfer coefficient, A_w is the effective heat convection area of the accumulator, and T_w is the accumulator wall temperature. For a real gas, u can be described as

$$du = c_v dT + \left[T\left(\frac{\partial p_g}{\partial T}\right)_v - p_g\right]dv, \tag{4}$$

where c_v is the constant-volume specific heat of gas. It should be noted that c_v is gas temperature T and specific volume v dependent

$$c_v = c_v^0 + \frac{6}{T^3}\left(\frac{C_0}{v} - \frac{c}{\gamma}\right) + \frac{3c}{T^3}\left(\frac{2}{\gamma} + \frac{1}{v^2}\right)e^{-\gamma/v^2}, \tag{5}$$

where C_0, c, and γ are constants in BWR equation, and c_v^0 is the constant-volume specific heat for ideal gas. Generally, c_v^0 also varies with the gas temperature T. However, for nitrogen used in this analysis, the change is so small during the normal working temperature range and constant c_v^0 can be used.

Combining (2), (3), and (4) yields [15].

$$\left(1+\frac{m_f c_f}{m_g c_v}\right)\frac{dT}{dt}=\frac{T_w-T}{\tau}-\frac{1}{c_v}\left[\frac{RT}{v}\left(1+\frac{b}{v^2}\right)+\frac{1}{v^2}\left(B_0RT+\frac{2C_0}{T^2}\right)-\frac{2c}{v^3T^2}\left(1+\frac{\gamma}{v^2}\right)e^{-\gamma/v^2}\right]\frac{dv}{dt}, \tag{6}$$

with a thermal time constant of

$$\tau=\frac{m_g c_v}{hA_w}. \tag{7}$$

Obtaining v from (1), the gas temperature can be calculated by (6). Then, gas absolute pressure p_g can be obtained by (2).

The pressure difference between p_a and p_g is the pressure loss caused by the friction, e.g. flow entrance effects, viscous shear, etc. Detailed modelling of friction loss is possible but its magnitude does not justify the complexity it brings into the analysis. To simplify the model, the pressure loss (as percentage of the fluid pressure p_a at accumulator inlet) is assumed to be half of the friction loss (as percentage of input L_f/E), as

$$\frac{p_g-p_a}{p_a}=\operatorname{sgn}(dV)\frac{k}{2}\frac{L_f}{E}, \tag{8}$$

where $\operatorname{sgn}(dV)=\begin{cases}+1 & \text{fluid outflow}\\ -1 & \text{fluid inflow}\end{cases}$,

L_f is the accumulator friction loss in one cycle, E is the energy input to the accumulator in one cycle, and k is a factor introduced to avoid pressure jump when flow direction changes. A simple linear variation of k when flow direction changes is illustrated in Fig. 2.

2.2 Hydraulic motor/pump

Hydraulic motor/pump is an energy conversion device. It converts hydraulic energy to mechanical energy when operating in motor mode, and mechanical energy to hydraulic energy while operating in pump mode. Thus, it has two interfaces: (a) from the hydraulic side where actual flow rate entering the hydraulic motor/pump Q_m and pressure difference between the inlet and outlet Δp are required; (b) from the mechanical side where actual torque T_m and angular velocity ω are needed.

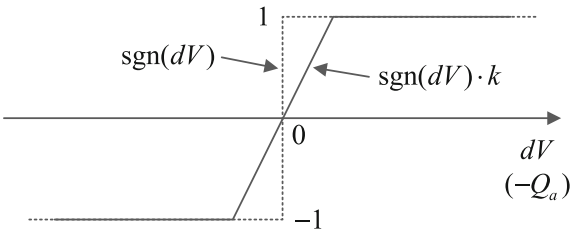

Fig. 2 Illustration of pressure drop coefficient

The ideal flow rate of the fluid entering the hydraulic motor/pump can be calculated by

$$Q_{mi}=x\omega D, \tag{9}$$

where D is the maximum motor/pump displacement per radian, ω is the angular velocity, and x is the fraction of maximum unit capacity. It is known that x is related to the swivel angle α_0 of the hydraulic motor/pump as [http://www.insanehydraulics.com/library/files/Hydraulic-Trainings-for-Axial-Piston-Units.pdf].

$$x=\frac{\sin\alpha_0}{\sin\alpha_{0,\max}}. \tag{10}$$

Swivel angle α_0 can be either positive or negative as the hydraulic motor/pump has two operation modes. It is defined in this analysis that the flow rate is positive in motor mode, which corresponds to positive swivel angle.

2.2.1 The volumetric efficiency

In reality, the ideal flow rate is always lower than the actual flow rate Q_m in motor mode, due to leakage, cavitation, and fluid compressibility. By neglecting the cavitation loss, which is small for modern hydraulic motor, the volumetric efficiency can be calculated as [15].

$$\eta_v=\frac{Q_{mi}}{Q_m}=\frac{1}{1+\frac{C_s}{x\,S}+\frac{\Delta p}{\beta}+\frac{C_{st}}{x\,\sigma}}, \tag{11}$$

where C_s and C_{st} are the laminar and turbulent leakage coefficients respectively, and β is the fluid bulk modulus of elasticity (1660 MPa for most hydraulic fluid). S and σ are given as.

$$S\equiv\frac{\mu\omega}{\Delta p},\ \text{and}\ \sigma\equiv\frac{\omega D^{1/3}}{(2\Delta p/\rho)^{1/2}}, \tag{12}$$

where μ is the fluid viscosity, and ρ is the fluid density.

2.2.2 The torque efficiency

The torque provided by an ideal hydraulic motor is

$$T_{mi}=x\,\Delta p\,D. \tag{13}$$

The motor torque efficiency may be calculated as [15].

$$\eta_t=\frac{T_m}{T_{mi}}=1-\frac{C_v S}{x}-\frac{C_f}{x}-C_h x^2\sigma^2, \tag{14}$$

where C_v, C_f and C_h are the viscous, frictional, and hydrodynamic loss coefficients, respectively. Then, the actual torque T_m provided by the hydraulic motor can be found, which is used to drive the electric generator.

Similarly, the equivalent equations for pump mode are

$$\eta_v=\frac{Q_m}{Q_{mi}}=1-\frac{C_s}{|x|S}-\frac{\Delta p}{\beta}-\frac{C_{st}}{|x|\sigma}, \tag{15}$$

$$\eta_t = \frac{T_{mi}}{T_m} == \frac{1}{1 + \frac{C_v S}{|x|} + \frac{C_f}{|x|} + C_h x^2 \sigma^2}. \quad (16)$$

2.3 Reservoir

The reservoir normally has a slightly higher pressure than the minimum intake pressure of the hydraulic motor/pump to ensure proper operation. A low-pressure accumulator with a relatively large volume is considered to serve this purpose in the analysis. Thus, the changing speed of the gas volume is relatively low during the operation, which means that the thermodynamic process can be assumed to be quasi-static and the gas can be treated as ideal. The gas thermodynamic process in the reservoir can be described by the Polytropic relationship

$$p_r V_r^n = \text{Constant}, \quad (17)$$

where p_r and V_r are the gas pressure and volume in the reservoir respectively, and n is heat capacity ratio. For a diatomic gas, such as nitrogen, $n = 1.4$ [16].

2.4 Pipeline

The main hydraulic components are connected by pipelines, including pipes, hoses, unions, fitting, bends, valves, etc. All these connecting elements have similar characteristics regarding the pressure loss, i.e. the loss is proportional to the square of the actual flow rate through the element. Thus, the total pressure loss in the pipelines Δp_p can be estimated by summing the "equivalent pipe length" of all elements

$$\Delta p_p = f \frac{L_p}{D_p} \frac{\rho}{2} \frac{Q_p^2}{A_p^2}, \quad (18)$$

where f is the friction coefficient, L_p is the total effective pipe length, D_p and A_p are the equivalent pipe internal diameter and cross-sectional area respectively, and Q_p is the flow through the pipelines.

The friction coefficient f is related to the fluid velocity through the pipelines. When the fluid velocity is high enough, the flow in the pipelines becomes turbulent flow instead of laminar flow. Reynolds number is used to judge the flow type

$$\text{Re} = \frac{4\,|Q_p|}{\pi\, D_p\, \nu}, \quad (19)$$

where ν is the fluid kinematic viscosity. For laminar flow

$$f = 64/\ \text{Re}, \quad \text{Re} \le 2000. \quad (20)$$

While for turbulent flow

$$f = 0.332\ \text{Re}^{-1/4}, \quad 2000 < \ \text{Re} \le 10^5. \quad (21)$$

2.5 Electrical generator

The generator converts the mechanical energy from the hydraulic motor to electrical energy. A Surface-Mounted Permanent Magnet Synchronous Generator (SM-PMSG) is chosen to simplify the analysis as well as achieving high energy efficiency. The machine torque equation is

$$T_e = \frac{n_{ph}}{2} p \lambda_{pm} I_s \cos\phi_i, \quad (22)$$

where T_e is the machine electromagnetic torque, n_{ph} is the number of phases, p is the number of pole-pairs, λ_{pm} is the flux linkage from the permanent magnets, I_s is the machine current amplitude, and ϕ_i is the internal power factor angle (angle between current and internal voltage).

To use the machine current effectively, the machine current vector angle is controlled to achieve unit internal power factor, i.e. $\cos\phi_i = 1$. Thus, I_s can be obtained according to (22) for certain T_e. Then, the machine copper loss can be calculated as

$$p_{Cu} = 0.5 n_{ph} I_s^2 R_s, \quad (23)$$

where R_s is the machine phase resistance.

At certain machine rotary speed n_r, the corresponding machine electrical frequency f_s can be calculated as

$$f_s = p \cdot n_r / 60. \quad (24)$$

The machine iron loss includes the hysteresis loss and eddy current loss, which are proportional to f_s and f_s^2, respectively. Then, the generator energy efficiency can be calculated as

$$\eta_g = \frac{P_{out}}{P_{in}} = \frac{T_e \omega_r - p_{Cu} - C_{hys} f_s - C_{edy} f_s^2}{(T_e + B_m \omega_r)\omega_r}, \quad (25)$$

where B_m is the machine viscous friction coefficient, C_{hys} and C_{edy} are the hysteresis and eddy current loss coefficients, respectively.

2.6 System integration

To integrate the above main components and form the hydraulic system illustrated in Fig. 1, the following rules should be complied with.

2.6.1 The continuity equation

The effective flow rate Q_e is equal to the sum of the actual flow rates entering the accumulator Q_a and the hydraulic motor Q_m

$$Q_e = Q_a + Q_m. \quad (26)$$

The effective flow rate Q_e is equal to the system input flow rate Q_{in} when relief valve is not activating

$$Q_e = \begin{cases} Q_{in} & \text{, when } p_a < p_{a,\max} \\ Q_m & \text{, when } p_a \geq p_{a,\max} \end{cases} \quad (27)$$

2.6.2 Pressure balance

The pressure difference between the accumulator and reservoir is equal to the pressure drop on the hydraulic motor and pipelines

$$\Delta p = p_a - p_r - \operatorname{sgn}(\alpha_0)\,\Delta p_p. \quad (28)$$

where

$$\operatorname{sgn}(\alpha_0) = \begin{cases} +1 & \text{motor mode} \\ -1 & \text{pump mode} \end{cases}. \quad (29)$$

2.6.3 The equation of motion

The connection between the hydraulic motor and electrical generator should follow the motion equation as

$$T_m = J\frac{d\omega_r}{dt} + B_m\omega_r + T_e. \quad (30)$$

where J is the total moment of inertia of the rotary parts of the hydraulic motor and electrical generator.

3 System implementation

The HESC system can either be integrated into the PTO system or be included as a subsystem of the WEC. Fig. 3a illustrates a typical PTO system (e.g. a float module of a PA-WEC) integrated with a HESC system. The bi-directional flow obtained from the symmetric cylinder is converted to unidirectional flow by e.g. a hydraulic "H-bridge rectifier" consisted of four non-return valves. Then the unidirectional flow serves as the input of the HESC system. In addition, the HESC system could be integrated as a subsystem of the WEC as shown in Fig. 3b, so that the hydraulic motor and generator used in the PTOs are not oversized [8].

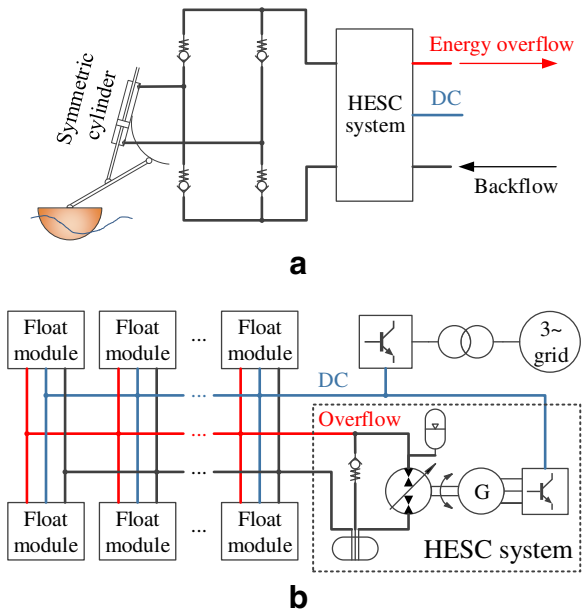

Fig. 3 PTO system with HESC system integrated. **a** Float module with HESC system. **b** HESC subsystem handling the overflow energy of PTOs

A PTO system integrated with HESC system is studied in this paper. Fig. 4 shows the extracted power profile, which is optimized by certain Wave Power Extraction Algorithm (WPEA) [8]. It corresponds to the power profile that the PTO system of Wavestar WEC [11] can extract from sea state 3, which has large waves. While sea state 1 and 2 correspond to small and medium wave conditions, respectively.

When knowing the extracted power from the cylinder P_{in}, the system input flow rate can be calculated as

$$Q_{in} = P_{in}/p_a, \quad (31)$$

where p_a is the accumulator inlet pressure.

3.1 Control strategy

It is seen from Fig. 4 that the harvested wave energy has a period around 3 s, which is much longer than the electrical time constant of a generator. Therefore, it is justifiable to state that the hydraulic motor and the electrical generator can be controlled to operate at a constant speed, e.g. the synchronous speed of the generator.

Due to the facts that the system input flow rate varies as the input wave energy fluctuates (31) and the storage capability of the accumulator is limited, the flow rate used to drive the hydraulic motor should be well adjusted to ensure smooth power output. Variable-displacement control of the hydraulic motor, which is achieved by varying the fraction of maximum unit capacity x defined in (10), can be adopted for constant speed drive.

From the storage capacity point of view, a feasible and direct indication signal can be the fluid level in the accumulator, which can be transformed to the gas volume V. The control strategy of x could be:

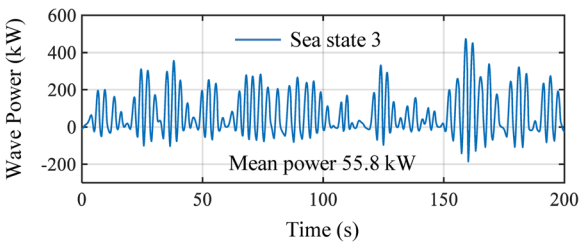

Fig. 4 Power profile at sea state 3, for the WaveStar [11]

(a) when V reaches its maximum allowable volume $V_{\max}$, no more fluid is allowed to flow out of the accumulator and x is set to zero;
(b) when V is below a pre-set value V_{pre} (e.g. 80% of $V_{\max}$), x is set to one to enable maximum output;
(c) when V is between V_{pre} and $V_{\max}$, x is given by

$$x = \frac{V_{\max} - V}{V_{\max} - V_{pre}}. \tag{32}$$

However, the above control strategy of x may result in overloading of the generator. Therefore, power control should be taken into account as well. A simple proportional-integral (PI) regulator is used to adjust the maximum allowable x, where the rated torque of the generator (or the rated phase current amplitude) is set as the reference. The minimum value of x obtained from storage capacity control and torque/current control is chosen when driving the hydraulic motor.

3.2 System configuration

The parameters of the gas accumulator, hydraulic motor, and generator used in the analysis are given in Tables 1, 2 and 3, respectively.

Eight gas accumulators are connected in the HESC system to provide enough storage capability. The mass of gas in the reservoir is 2 kg with a pressure of 0.394 MPa. The total effective pipe length and the equivalent pipe internal diameter are estimated to be 12 m and 0.015 m, respectively. The fluid in the system is oil with the density and kinematic viscosity of 869 kg/m^3 and 60×10^{-6} m^2/s, respectively.

3.3 System operation performance

Figure 5 shows the HESC system operation performance at sea state 3. It can be seen that the system pressure is controlled and limited to the maximum allowable value of the accumulator inlet absolute pressure (i.e. 21 MPa as listed in Table 1). When the input wave energy exceeds the system's capability (e.g. during time range of 24 s to 28 s), the relief valve activates and the flow entering the accumulator is zero. Moreover, it can be observed from the time interval 29~ 33 s that the generator output power is well controlled and limited to its rated power (i.e. 35 kW). When the system pressure is about 18 MPa at 29 s, the fraction of maximum unit capacity x of the hydraulic motor is one to maximize its output. Due to the surge input, the output power of the hydraulic motor increases as the system pressure increases. Thus, x is adjusted by the controller to limit the hydraulic motor shaft output, so that the generator will not exceed its rated value. It can be seen that the energy efficiency of the HESC system itself is around 61.7%. While for the whole system, where the overflow is considered as loss, the energy efficiency is about 53.2%.

Table 1 Gas accumulator parameters [17]

Mass of Gas	1.213 kg	Max. Gas Volume	15.271×10^{-3} m^3
Mass of Foam	1.496 kg	Foam Specific Heat	2300 J/kg·K
Friction Loss	4%	Gas Constant	8.31446 J/K/mol
Max. Pressure	21 MPa	Thermal Time Const.	300 s

Table 2 Hydraulic motor parameters [17]

Displacement	107 cm^3/rev	Max. Swivel Angle	25 deg
Friction Coef.	0.0048	Laminar Leakage Coef.	1.042×10^{-9}
Viscous Coef.	153,407	Turbulent Leakage Coef.	1.20×10^{-5}
–	–	Hydrodynamic Loss Coef.	0

4 Design optimization

The efficiency of the example system shown in Fig. 5 is not very satisfactory. Thus, investigation into the design of the system ratings is carried out in this section to optimize the system energy efficiency.

Figure 6 shows the system energy efficiency with different system rating configurations at 21 MPa system pressure with generator power rating varying from 30 kW to 40 kW. It can be seen from Fig. 6a that the HESC system efficiency increases as the maximum hydraulic motor/pump displacement D decreases in a wide range (40 to 120 cm^3/rev). However, the maximum accumulator gas volume $V_{\max}$ (storage capacity) has limited influence on the HESC system efficiency. This is because that the energy overflow is not considered as losses of the HESC system, since it could be handled by another HESC system as shown in Fig. 3b. However, such assumption will result in unreasonable small system capacity, since small D means small torque (13). Thus, the whole system efficiency should be taken into account when performing design optimization. It can be seen in Fig. 6b that there is an optimal D value (around 100 cm^3/rev), which can provide higher whole system efficiency.

Figure 6c shows the whole system efficiency at sea state 2, where medium wave condition presents and less

Table 3 Generator parameters

Rated Power	35 kW	Phase Resistance	0.1625 Ω
Rated Voltage	380 V	PM Flux Linkage	1.035 Wb·t
Rated Current	54.26 A	Rated Efficiency	93.5%
Rated speed	1500 rpm	Rated Power Factor	0.98
No. of Phases	3	Hysteresis Loss Coef.	9.4893
No. of Poles	4	Eddy Current Loss Coef.	0.1898
Rotor Inertia	0.0885 kg·m^2	Viscous friction Coef.	0.0020

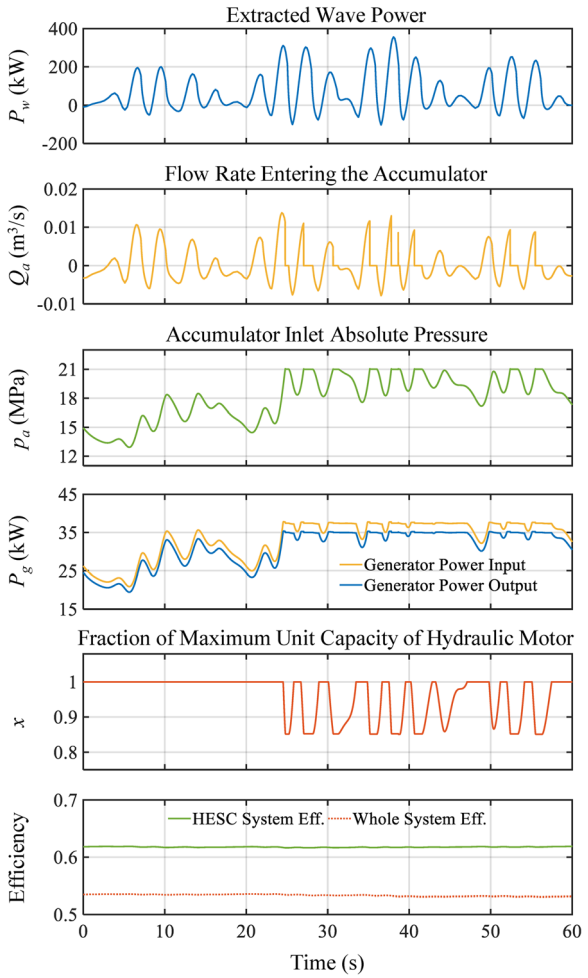

Fig. 5 HESC system operation performance at sea state 3

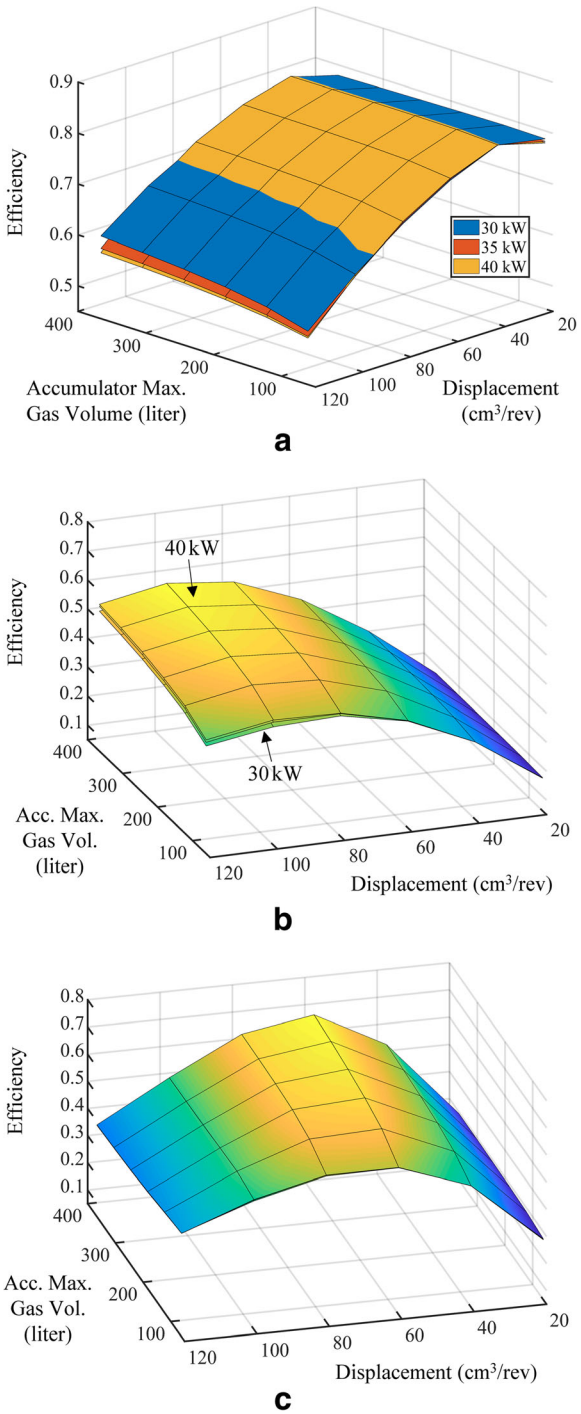

Fig. 6 System energy efficiency at 21 MPa system pressure with different generator power ratings. **a** HESC system efficiency at sea state 3. **b** Whole system efficiency at sea state 3. **c** Whole system efficiency at sea state 2

energy can be extracted. It can be seen that the optimal D value to achieve best whole system efficiency is reduced to around 60 cm^3/rev. This is reasonable since the average wave power is reduced, and a system with power ratings close to the wave power level could provide higher energy efficiency.

Moreover, rather than the HESC system efficiency shown in Fig. 6a, the whole system energy efficiency is dependent on the accumulator storage capacity V_{max}. Large V_{max} will certainly help to increase the system efficiency as shown in Fig. 6b and c. Furthermore, the generator power rating, which can be considered as the system power rating, will also influence the system efficiency. However, the influence is small as can be seen in Fig. 6a though higher power rating is likely to give slightly higher system efficiency when the system is properly designed.

4.1 Influence of system pressure

It has been observed from Fig. 6a that small D can help to increase the HESC system efficiency. However, small D will reduce the system power rating (13), and the whole system efficiency is decreased due to large amount of energy overflow. A straightforward way is to increase the system pressure. According to (13), D can

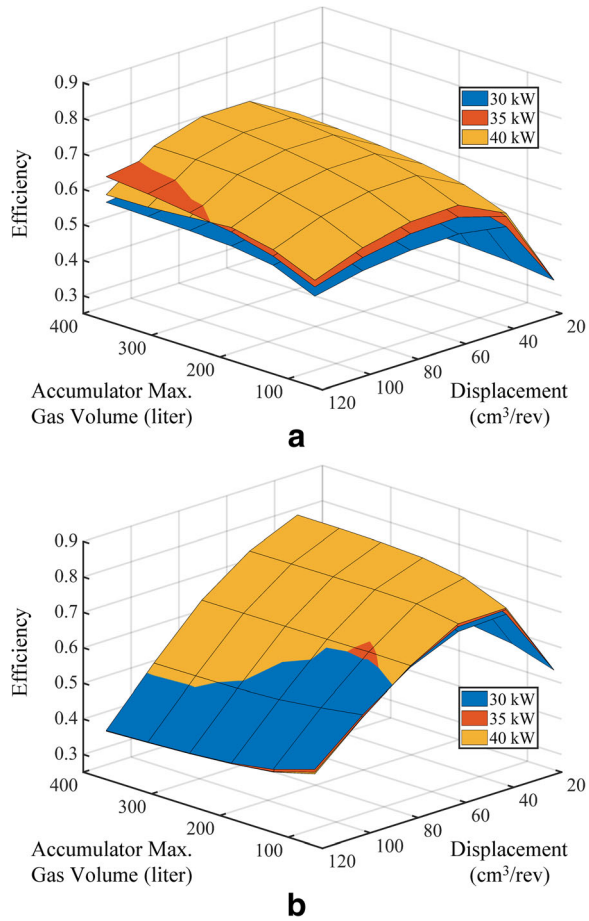

Fig. 7 Whole system energy efficiency at 42 MPa system pressure. **a** At sea state 3. **b** At sea state 2

be halved when Δp is doubled. Fig. 7 shows the whole system energy efficiency when the system pressure is 42 MPa. It can be seen that the whole system efficiency for both sea state 2 and 3 can be balanced when D is around 50 cm^3/rev, which is about half of the original D in Table 2.

Compared with the system efficiency at 21 MPa, the energy efficiency increases from 59.8% to 74.0% for sea state 3, from 71.1% to 82.3% for sea state 2. Furthermore, it can be observed that the system storage capacity has its saturation value of around 300 l at sea state 2; while the system efficiency can still be improved by increasing the storage capacity at sea state 2 when 21 MPa system pressure is applied. Thus, increasing the system pressure will help to increase the system efficiency and reduce the system storage capacity required.

Further increase to the system pressure could be considered to achieve slightly higher energy efficiency, e.g. 76.9% and 83.2% for sea state 2 and 3 respectively at 63 MPa. However, the cost of high-pressure devices increases as the pressure rises. Detailed evaluation is needed to find the optimal system pressure, so that the most economical system solution can be obtained.

5 Conclusion

In this paper, a HESC system for WECs is introduced and modelled in details. Control strategy is proposed to ensure that all the components are operating properly within their maximum limits. A case study of the HESC system is provided to evaluate the proposed control strategy and the system efficiency by taking the power profile of the WaveStar project as an example. Design investigation of the HESC system is then carried out to optimize the system energy efficiency. It is found that increasing the system pressure will help to increase the system efficiency and reduce the required optimal system storage capacity although the cost of high-pressure components will also increase. The balance between the system cost and payback of extra energy harvest should be carefully evaluated. The analysis carried out in this paper can be used to achieve the optimal system design of the HESC system.

Authors' contributions

DW carried out the design of the study, developed the system model, performed the system design investigation and optimization, analyzed the data, and drafted the manuscript. KL initialized the problem, coordinated the resources, participated in the design and data analysis, and helped to draft the manuscript. All authors read and approved the final manuscript.

Competing interests

The authors declare that they have no competing interests.

Received: 28 September 2017 Accepted: 31 January 2018
Published online: 12 March 2018

References

1. Muetze, A., & Vining, J. G. (2006). Ocean wave energy conversion - a survey. Industry Applications Conference - 41st IAS Annual Meeting, 3, 1410–1417.
2. Drew, B., Plummer, A. R., & Sahinkaya, M. N. (2009). A review of wave energy converter technology. *Proc of The Institution of Mechanical Engineers, Part A-journal of Power and Energy, 223*(8), 887–902.
3. Falcao, A. F. de O. (2010). Wave energy utilization: A review of the technologies. *Renew Sust Energ Rev, 14*(3), 899–918.
4. Dorrell, D. G., Halliday, J. R., Miller, P., & Findlater, M. (Sep. 2004). *"Review of wave energy resource and oscillating water column modelling," 39th international universities power Eng Conf* (Vol. 1, pp. 649–653).
5. Kofoed, J. P., Frigaard, P., Friis-Madsen, E., & Sorensen, H. C. (2006). Prototype testing of the wave energy converter wave dragon. *Renew Energy, 31*, 181–189.
6. Vicinanza, D., Margheritini, L., Kofoed, J. P., & Buccino, M. (2012). The SSG wave energy converter: Performance, status and recent developments. *Energies, 5*(2), 193–226.
7. Polinder, H., Damen, M., & Gardner, F. (Sept. 2004). Linear PM generator system for wave energy conversion in the AWS. *IEEE Transactions on Energy Conversion, 19*(3), 583–589.
8. Hansen, R. H., Andersen, T. O., & Pedersen, H. C. (2011). Model based Design of Efficient Power Take-off Systems for wave energy converters. *The Twelfth Scandinavian International Conference on Fluid Power, 2*, 35–49.
9. Tedeschi, E., Carraro, M., Molinas, M., & Mattavelli, P. (2011). Effect of control strategies and power take-off efficiency on the power capture from sea waves. *IEEE Transactions on Energy Conversion, 26*(4), 1088–1098.
10. Holm, R. K., Berg, N. I., Walkusch, M., Rasmussen, P. O., & Hansen, R. H. (2013). Design of a magnetic lead screw for wave energy conversion. *IEEE Transactions on Industry Applications, 49*(6), 2699–2708.
11. Wave Star A/S. http://www.wavestarenergy.com.
12. AWS Ocean Energy Ltd. http://www.awsocean.com.

13. Weinstein, A., Fredrikson, G., Parks, M. J., & Nielsen, K. (2004). AquaBuOY - the offshore wave energy converter numerical modeling and optimization. Proceedings of MTTS/IEEE Techno-Ocean'04, 4, 1854–1859.
14. Sabzehgar, R., & Moallem, M. (2009). A review of ocean wave energy conversion systems. Proceedings IEEE Electrical Power Energy Conference (EPEC),1, pp. 1–6.
15. Pourmovahed, A., Beachley, N. H., & Fronczak, F. J. (Mar. 1992). Modeling of a hydraulic energy regeneration system – Part I: Analytical treatment. *J Dyn Syst Meas Control, 114*, 155–159.
16. White, F. M. (2009). *Fluid Mechanics* (7th ed.p. 827). New York: McGraw Hill.
17. Pourmovahed, A., Beachley, N. H., & Fronczak, F. J. (Mar. 1992). Modeling of a hydraulic energy regeneration system – Part II: Experimental program. *J Dyn Syst Meas Control, 114*, 160–165.